Magnetization reversal in circular vortex dots of small radius

M. Goiriena-Goikoetxea[a], K.Y. Guslienko[b,c], M. Rouco[d], I. Orue[e], E. Berganza[f], M. Jaafar[f], A. Asenjo[f], M.L. Fernández-Gubieda[a,d], L. Fernández Barquín[g], and A. García-Arribas[a,d]

[a] *Basque Center for Materials, Applications and Nanostructures (BCMaterials), Parque Tecnológico de Bizkaia, Building 500, Derio, Spain. Tel: +34 946128811; mail: maite.goiriena@bcmaterials.net*

[b] *Department of Materials Physics, University of the Basque Country (UPV/EHU), 20018 Donostia, Spain*

[c] *IKERBASQUE, The Basque Foundation for Science, 48013 Bilbao, Spain*

[d] *Department of Electricity and Electronics, University of the Basque Country (UPV/EHU), 48940 Leioa, Spain*

[e] *SGIKER Magnetic Measurements, University of the Basque Country (UPV/EHU), 48940 Leioa, Spain*

[f] *Instituto de Ciencia de Materiales de Madrid, CSIC, 28049 Madrid, Spain.*

[g] *CITIMAC, University of Cantabria, 39005 Santander, Spain*

We present a detailed study of the magnetic behavior of Permalloy (Ni80Fe20 alloy) circular nanodots with small radii (30 nm and 70 nm) and different thicknesses (30 nm or 50 nm). Despite the small size of the dots, the measured hysteresis loops manifestly display the features of classical vortex behavior with zero remanence and lobes at high magnetic fields. This is remarkable because the size of the magnetic vortex core is comparable to the dot diameter, as revealed by magnetic force microscopy and micromagnetic simulations. The dot ground states are close to the border of the vortex stability and, depending on the dot size, the magnetization distribution combines attributes of the typical vortex, single domain states or even presents features resembling magnetic skyrmions. An analytical model of the dot magnetization reversal, accounting for the large vortex core size, is developed to explain the observed behavior, providing a rather good agreement with the experimental results. The study extends the understanding of magnetic nanodots beyond the classical vortex concept (where the vortex core spins have a negligible influence on the magnetic behavior) and can therefore be useful for improving emerging spintronic applications, such as spin-torque nano-oscillators. It also delimits the feasibility of producing a well-defined vortex configuration in sub-100 nm dots, enabling the intracellular magneto-mechanical actuation for biomedical applications

Introduction

The magnetic properties of materials at the nanoscale and the wide range of innovative applications that they disclose are absolutely compelling. The fields of nanomagnetism and spintronics are actively exploiting these properties with outstanding achievements.[1,2] A paradigmatic example of the paramount importance of size in magnetism is the absence of magnetic domains, which dominate the magnetization processes of macroscopic materials, in magnetic nanoparticles. In the single domain state, the exchange energy dominates and the magnetic nanoparticle behaves as a simple giant spin.[3] Increasing the particle size, the role of magnetostatic energy increases

and disc-shaped particles of adequate dimensions can display the so-called spin-vortex configuration, a kind of magnetic topological soliton stabilized in a restricted geometry.[4,5] The vortex state is characterized by the magnetic moments being curled in the plane of the dot, configuring closed circles to minimize the magnetostatic energy. Only at the dot center, at the core of the vortex, the magnetic moments get out of the plane and point perpendicularly, to avoid the singularity. The magnetic behavior as a function of the in-plane applied magnetic field is characteristic for vortex structures: at low fields, the vortex core is displaced reversibly in the plane until it reaches the dot lateral border, where it is annihilated and the sample becomes magnetically saturated. Reducing the magnitude of the applied field, the vortex is nucleated again, but at a magnetic field of lower intensity than the one of the annihilation, and then follows back the original reversible path. This originates a very peculiar hysteresis loop with no remanence or coercive field and open lobes at high fields,[6] as exemplified in the inset of Figure 1.

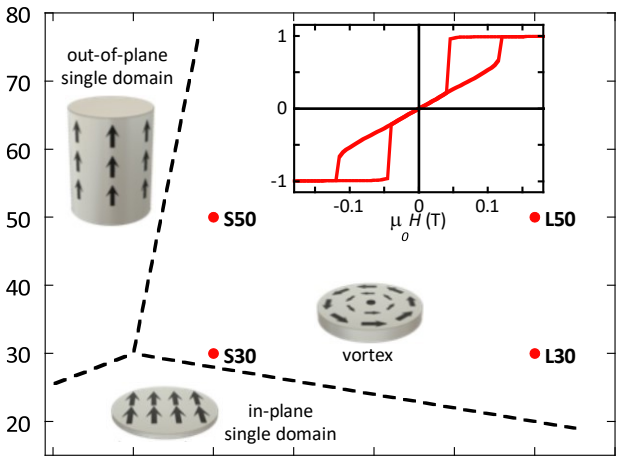

Figure 1. Schematic phase diagram of the magnetic ground state of Permalloy dots, as a function of their thickness and radius. The dashed lines separate the regions with different magnetic configurations and their position is sketched according to previous diagrams elaborated from experimental and theoretical results.[5,18-21] (When necessary, the value of the exchange length L_e = 5.7 nm, as provided in Ref. 5, has been used to scale the results). The arrows drawn in the cylinders reflect the configuration of the magnetization. The samples studied in this work are situated in the diagram by red dots, labelled according to the nomenclature introduced in Table I. The inset displays the shape of a typical hysteresis loop in the vortex state (obtained from a micromagnetic simulation).

The vortex magnetic arrangement possesses attractive features for very diverse applications. In magnetic information storage, the vortex spin configuration, is expected to display smaller thermal and quantum fluctuations than conventional systems, as it comprises many spins.[7] Vortex-state dots are also used as an active layer in the spin-torque nano-oscillators generating microwaves excited by a DC spin-polarized current.[8] Furthermore, vortex-state dots, dispersed in water, can act as magneto-mechanical actuators: the force generated by their oscillation in a low-amplitude and low frequency magnetic field is capable to damage the membrane of cancer cells[9,10] or to be used as drug delivery agents.[11] Smaller particles with the same magnetic characteristics would be promising because they could largely expand the application range. For all these applications, a detailed understanding of the magnetic features and the magnetization

processes of the dots with vortex-state becomes essential.

In micron-sized dots, the vortex state has been extensively studied, both experimentally, by different magnetometry techniques,[12] magnetic force microscopy (MFM)[13] or spin- polarized scanning tunneling microscopy (SP-STM),[14] and theoretically, using micromagnetic modelling[15] and fully analytical descriptions.[6] Typically, in micron-sized dots the core of the vortex occupies a negligible area of the dot, being about 20-30 nm wide, and therefore, its effect can be safely neglected in the description of the overall magnetic behavior. Despite its relevance, a very scarce number of works can be found on sub-100 nm vortex structures, mainly due to the difficulty of sample preparation and the limitations of the characterization techniques. A notable work on Fe dots with diameters down to 52 nm, prepared using alumina templates, reveals the existence of a transition from a single domain to vortex state depending on the dot diameter,[16] whereas the vortex core has a diameter of about 20 nm.[17] We have recently reported the preparation of 60 nm Permalloy ($Ni_{80}Fe_{20}$) dots by hole mask colloidal lithography (HCL) with a very well defined vortex state.[18] The determination of the nature of the magnetization processes in such structures ought to have a relevant role in their application in spintronic devices as well as in biomedicine where the particle reduced size favors the internalization by the cells.

We are especially interested in downsizing dot-shaped particles while maintaining the vortex configuration that allows the magneto-mechanical actuation. In this work, we present a complete study on the magnetization processes and the magnetic vortex characteristics of a set of Permalloy dots, prepared by HCL, with two different radii, 30 and 70 nm, and two different thicknesses, 30 and 50 nm. With a radius of 30 nm, according to the magnetic phase diagram (Figure 1), the variation of the aspect ratio of the dots can produce considerable changes in the magnetic ground state, evolving from the in-plane single domain to the vortex state and approaching to the boundary of the out-of-plane single domain as the thickness of the dot is increased. Therefore, the dots that we have selected, could delimit the region with a definite vortex configuration. The dots with a radius of 70 nm are expected to present a clear vortex configuration for both thicknesses, and are included in the study to help understanding the behavior of the dots with smaller size.

The precise morphology of the samples is determined by electron and atomic force microscopies (these results are available as the electronic supplementary information to the manuscript). Afterwards, we describe the magnetic measurements that reveal hysteresis loops with very well-defined vortex behavior. Magnetic force microscopy images could only be obtained in the dots having a radius of 70 nm, but they clearly show that the size of the vortex core is comparable to the size of the dot, a situation that has been predicted theoretically before and denominated *large vortex core*.[21] Micromagnetic simulations provide a description of the distribution of the magnetization in the dots. They confirm the existence of a large vortex core that, in dots with a radius of 30 nm, can be even larger than the dot itself (*extra-large vortex core*), depending on the thickness. The large vortex core notably influences the magnetic behavior of the nanostructures, but previous analytical descriptions of the magnetization reversal in vortex dots assume that the influence of the vortex core spins can be neglected due the

small core size.[6] Since this is no longer the case in small radius dots, a new analytical model is developed, whose predictions are shown to match reasonably to the experimental results. This model is finally used to discuss the magnetization reversal process of the dots having different radius and thickness.

Experimental

Sample description and morphological characterization

The nanodots were prepared by hole mask colloidal lithography (HCL).[18,22] Basically, this technique consists in creating an array of holes using polystyrene spheres as templates and filling them with the desired material. In our case, the dots were sputter-deposited from Permalloy ($Ni_{80}Fe_{20}$ alloy) targets onto Si wafers topped with a 400 nm SiO_2 layer. The HCL technique produces a dense but non-regularly distributed pattern of nanostructures, as illustrated in Figure 2. The diameter of the nanodots is mainly determined by the size of the polystyrene spheres used to create the template, whereas their thickness is controlled by the deposition time. Slight deviations beyond control in the multiple-step preparation process produce small differences between the nominal geometries and the ones obtained actually. Scanning electron microscopy (SEM, MEBFEG JEOL 7000F) and atomic force microscope (AFM, Nanotec Electrónica using the dynamic mode with a $Cr_{20}Au_{30}$ tip of 8 nm radius from MikroMasch) were used to perform the morphological assessment of the nanodots. The lateral size distribution was established by the analysis of SEM images using ImageJ software.[23] The thickness of the dots was determined from AFM profiles. The complete morphological characterization is presented as electronic supplementary information. Note that some of the samples are capped with a thin gold layer (3 or 4 nm) that does not interfere with the magnetic measurements. Table I identifies the magnetic nanostructures studied in this work and complies the relevant morphological data about them.

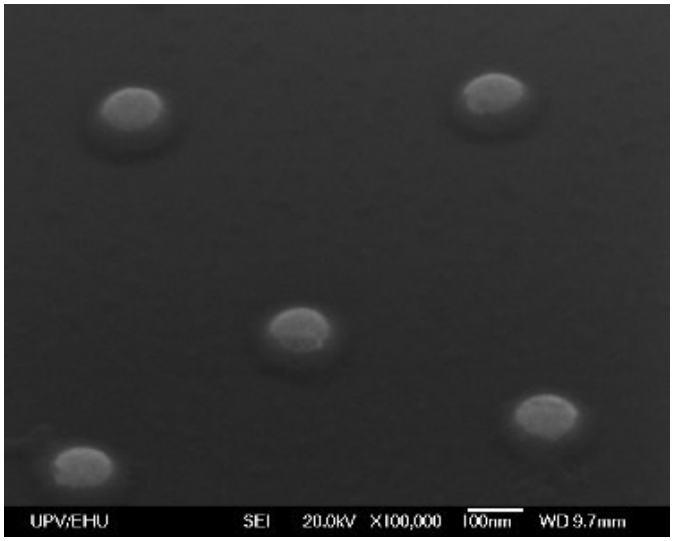

Figure 2. SEM image of $Ni_{80}Fe_{20}$ nanodots prepared by hole mask colloidal lithography corresponding to the sample L50, with a nominal radius R = 70 nm and thickness T = 50 nm.

Table I. Sample identification and morphological data (*R* = radius, *T* = thickness) of the Permalloy nanodots studied in this work.

Sample label	Nominal size		Real size[1]	
	R (nm)	***T*** (nm)	***R*** (nm)	***T*** (nm)
S30	30	30	35 ± 3	28 ± 1
S50	30	50	31 ± 3	52 ± 1
L30	70	30	73 ± 3	33 ± 1
L50	70	50	73 ± 3	53 ± 1

[1]Uncertainty in *R* corresponds to the standard deviation σ of the size distribution. The uncertainty in *T* is an estimated upper limit.

Magnetic characterization

The hysteresis loops measured either by superconducting quantum interference device (SQUID) or magneto-optical Kerr effect (MOKE) provide experimental information about the magnetization reversal mechanism in the nanostructures. SQUID measurements, with a sensitivity of the order of 10^{-11} Am^2, average the contribution of about 5×10^7 nanodots whereas the 20 μm wide laser spot used in the MOKE system collects information from about 10^3 dots. The loops obtained by both methods are very similar, confirming the homogeneity of the properties of the dots over the whole patterned surface. The MFM measurements were performed with a scanning force microscope from Nanotec Electrónica in the amplitude modulation mode, oscillating 12 nm and with a typical retrace lift of 20 nm. A second feedback loop, phase lock loop (PLL), was enabled to keep the maximum amplitude and make the phase zero. MFM probes (Nanosensors PPP-FMR) were laterally coated with 40 nm of Cobalt in a home-made built sputtering.

Experimental Results

The measured hysteresis loops for the dots having a radius of *R* = 30 nm are presented in Figure 3. It is especially significant that they definitely present the characteristic shape produced by the vortex configuration and its magnetization reversal process, displaying negligible coercivity, large permeability at zero field and hysteretic lobes at higher fields. Previous experimental evidence of the vortex behavior in these range of dimensions have not produced such perfectly shaped loops.[16,24] Dots with the same lateral diameter but thinner (*T* = 20 nm) present a definite in-plane single domain behavior as shown in the inset of Figure 3.*a*, in accordance with the magnetic phase diagram (Figure 1). The dots with *T* = 30 nm (Figure 3.*a*), although in definite vortex state, are close to the transition to in-plane single domain behavior. In fact, their hysteresis loop hints some reminiscence of single domain behavior by the presence of some remanence in the loop. In the results reported for slightly larger and thinner Permalloy dots (97 nm in diameter and 26 nm thick), this mixed behavior is much more evident and were attributed to the existence of an intermediate metastable state between in-plane single domain and vortex.[12] On the contrary, the dots with *T* = 50 nm (Figure 3.*b*) display the features of the vortex state with no remanence. However, the loop presents a marked slanted shape that deviates from the canonical vortex shape depicted in the inset of Figure 1. The slanted shape is especially evident by the fact that there is no sharply defined annihilation field and also because the regime of the loop that should remain at saturation until the vortex is nucleated back

does not present a constant value. This behavior evidences a mixture of magnetization mechanisms. The main characteristics of the vortex magnetization reversal prevail, but there is also some degree of coherent rotation of the magnetization, indicating the existence of a significant out-of-plane component of the magnetization (to support this assertion, the inset of Figure 3.b display the loop of an ideal monodomain spheroidal particle in which the magnetization reversal takes place completely by coherent rotation). This result is clearly a consequence of the closeness of this sample in the phase diagram to the region of the stable out-of-plane single domain state.

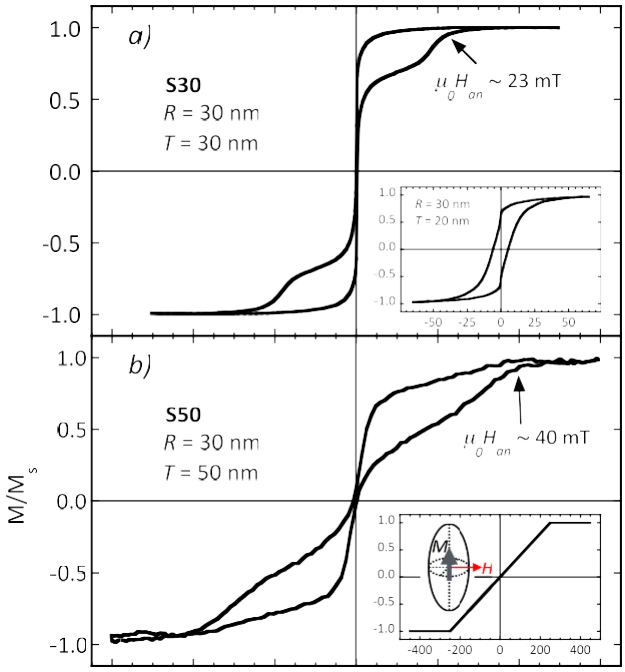

Figure 3. Hysteresis loops of $Ni_{80}Fe_{20}$ nanodots with nominal radius of $R = 30$ nm.

a) SQUID loop of sample S30 with a thickness $T = 30$ nm. The inset shows the loop measured in a sample with $T = 20$ nm, displaying a in-plane single domain behaviour.

b) MOKE loop of sample S50 with a thickness $T = 50$ nm. The inset represents the magnetization curve of an ideal out-of-plane monodomain spheroidal particle in which the magnetization reversal takes place by coherent rotation.

Figure 4 displays the hysteresis loops measured in the dots with $R = 70$ nm. For both samples with different thicknesses $T = 30$ nm and $T = 50$ nm, the shape of the hysteresis loop is the canonical one corresponding to the classical vortex behavior (the finite remanence and coercivity present in the SQUID measurement plotted in Figure 4.a come from a non- representative, badly patterned part of the sample, probably at the border of the substrate, since it is not present in the loop measured by MOKE, shown in the inset). Note that the central linear part of the loop in Figure 4.*b* presents certain similitude with the loop in the inset of Figure 3.*b*, but this is only a coincidence, since the magentization processes are completely different.

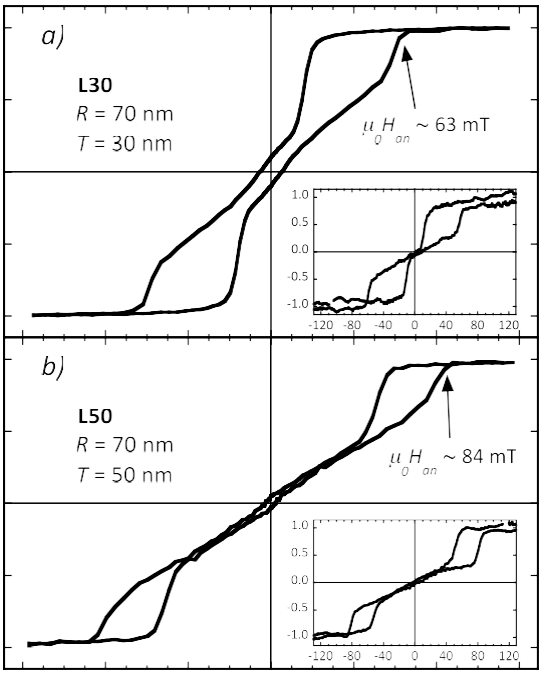

Figure 4. Hysteresis loops of $Ni_{80}Fe_{20}$ nanodots with nominal radius of R = 70 nm.
a) SQUID loop of sample L30 with a thickness T = 30 nm.
b) SQUID loop of sample L50 with a thickness T = 50 nm.
The insets show the MOKE loops measured in the same samples.

The value of the annihilation field H_{an} is indicated in Figures 3 and 4 for the dots with different sizes. It corresponds to the value of the applied field at which the vortex is expelled from the dot and the sample becomes magnetically saturated. From the experimental curves, it is determined with an estimated uncertainty of about ± 2 mT, since the saturation does not take place sharply. The annihilation field is an important parameter to test the validity of theoretical models, since H_{an} can be calculated analytically by energy minimization as the value of the in-plane magnetic field at which the core center reaches the border of the dot. In micron-sized dots, where the dimension of the vortex core can be neglected, the modelling produces quite accurate results.[6]

Figure 5 shows the MFM image obtained in the sample L50 (R = 70 nm and T = 50 nm), revealing the initial magnetic state of three nanodots. The vortex cores can be clearly observed as black or white spots in the center of the dots, depending if the magnetization at the core points up or down. For this sample, additional MFM images have been recorded under in-plane magnetic fields, showing the displacement of the vortex towards the edge of the dot. The images, shown in the electronic supplementary information accompanying this work, nicely correspond to the magnetic states revealed in the hysteresis loop. It is considerably challenging to obtain high- quality MFM images in such small structures. In this case, homemade Co coated tips were specifically prepared for these measurements to avoid modifications caused by the high stray fields coming from commercial MFM tips.[25,26] The image shown in Figure 5 is clear enough to estimate the radius of the vortex core R_C to be about half of the dot radius: $R_C \sim 30$ nm.

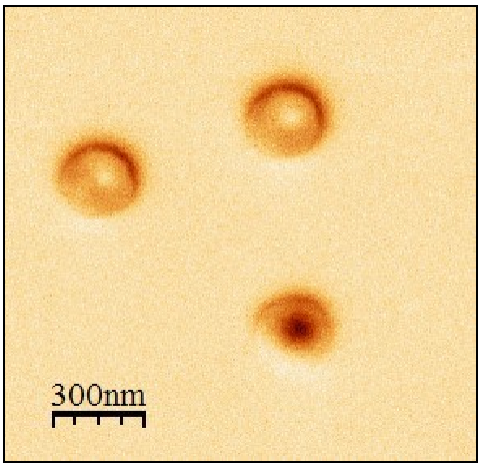

Figure 5. Magnetic force micrograph of $Ni_{80}Fe_{20}$ nanodots prepared by hole-mask colloidal lithography (nominal radius R = 70 nm and thickness T = 50 nm) at the initial magnetic state with the vortex cores at the centre of the dots pointing up or down (black or white).

Vortex structure from micromagnetic simulations

To complement the experimental results and to gain insight in the magnetic behavior of the small vortex dots, we have performed micromagnetic simulations in dots of the same geometries. Basically, the micromagnetic simulations solve the magnetization equation of motion and can calculate the complete behavior of the sample as a function of the applied field (in fact, the inset in Figure 1 has been obtained in this way). Here, we are interested in obtaining the configuration of the magnetization in the ground state, at zero applied field, to analyze the structure of the vortex. The simulations were performed with the OOMMF code,[27] using typical Permalloy parameters. The details of the calculation are given in the Methods section, below. Figure 6 represents the calculated out-of-plane component of the magnetization m_z as a function of the radial coordinate ρ, measured from the center of the dot (m_z is the reduced value of the magnetization M_z/M_s, being M_s the saturation magnetization). The actual magnetization can be slightly different along the thickness of the dot, so Figure 6 represents, for each radial position, the value of m_z averaged along the dot thickness. In a classical magnetic vortex, the magnetization is curled in the plain (m_z = 0), and only at the center, in the vortex core, it points perpendicularly. In the results of Figure 6, the radius of the vortex core R_C can be identified as the radial coordinate where m_z vanishes, *i.e.*, $m_z(R_C) = 0$. The simulation results show that m_z can also be negative, indicating that the individual moments are not perfectly in-plane even out of the vortex core. The determination of the core size by the criteria $m_z = 0$ is therefore affected by some uncertainty. Considering the magnitude of the negative mz values, we can estimate the uncertainty in the determination of Rc to be about 3 to 6 nm. The values of Rc are compiled in Table II. In any case, the simulation results clearly confirm that, in all the geometries, the vortex core extends up to a distance of the order of 30 nm from the dot center. This is in very good agreement with the MFM results, at least for the dots with R = 70 nm, where MFM images could be obtained. The size of the vortex core Rc is comparable to radius of the dot R. This situation is denominated large vortex core, in contrast with the situation of negligibly small vortex core Rc << R, occurring in micron- sized dots, designated as classical vortex. What is definitively remarkable is that, for the small dots with radius R = 30 nm, the vortex core extends

to the border of the dot. In the case of sample S50, the core seems to be even larger that the dot (Rc > R), which we call extra-large vortex core, but this situation does not prevent the existence of well-defined vortex-like reversal behavior as evidenced in the hysteresis loops displayed in Figure 3. The color profiles embedded in Figure 6 provide a descriptive illustration of the size and shape of the core of the vortex in the different dots. They correspond to the distribution of m_z values in the plane situated at half height of the dots.

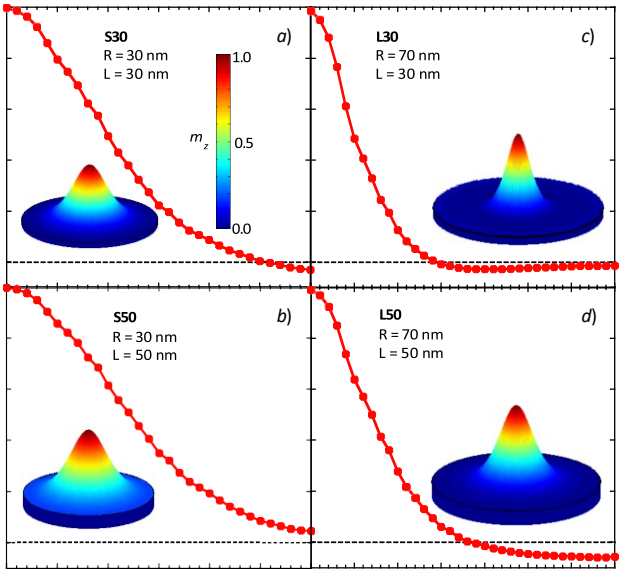

Figure 6. Radial dependence of the *z*-component of the magnetization, obtained from micromagnetic simulations. The curves represent the value averaged over the thickness of the dot. The colour profiles are created form the m_z values in the plane situated at half height of the dots.

The magnetization profiles represented in Figure 6 deserve a last remark. The negative values of m_z present in the samples S30, L30, and L50 recall the situation encountered in Bloch magnetic skyrmions,[28] in which the magnetization points in opposite directions between the core and the outer part of the structure. In this sense, the magnetization configuration in the large vortex core dots appears to be evolving from a classical vortex to a situation that recalls a Bloch-skyrmion configuration (it should be reminded here that the latter is n3 to 6 nmot supposed to be stable in Permalloy dots, with no Dzyaloshinskii-Moriya interaction and null perpendicular anisotropy).[28]

Model of magnetization reversal in the large vortex case

The large vortex core situation encountered experimentally and confirmed by the simulation results, cannot be described within the analytical approach for the classical (R_C << R) vortex magnetization reversal, developed in Ref. [6]. A revised theory is needed for sub-100 nm dots, where the vortex core is large compared with the size of the dot. The detailed theoretical description is given in the Methods section below. Here, we only outline the most relevant aspects and results. In particular, we present the expression that the model gives for the annihilation field H_{an} as a function of the parameter $c = R_C/R$, the vortex core radius relative to the radius of the dot, since H_{an} can be directly compared with experimental results.

As the distances between the dots are much larger than their diameter for all the samples, we assume that the dipolar inter-dot interaction is negligibly small in comparison with the in-dot magnetic energies.[29] Therefore, the problem of the magnetization reversal of a dot array is reduced to the problem of the magnetization reversal of a single circular dot of given radius R and thickness T.

The magnetic energy density (per unit of the dot volume $V = \pi R^2 T$) can be written as

$$w = A(\nabla m_\alpha)^2 - \frac{1}{2} M_s \mathbf{m}\mathbf{H}_\mathbf{m} + w_H \qquad (1)$$

where A is the exchange constant (which quantifies the strength of the magnetic interaction), $\alpha = x, y, z$, $\mathbf{m} = \mathbf{M}/M_s$ is the unit magnetization vector, $\mathbf{H_m}$ is the magnetostatic field, and w_H is the Zeeman energy density in an in-plane magnetic field.

The different terms in (1) can be calculated (see Methods) for the case of $c = R_C/R > 1$ (extra-large core) to obtain the energy $W(c, s, H)$ as a function of c, the position of the vortex core in the plane of the dot (represented by s in reduced coordinates) and the applied field H. The minimization of the energy $\partial W/\partial s = 0$ gives the equilibrium position s_0 of the vortex core for each applied field. The vortex annihilation field is then obtained as the field at which the position of the core equals the radius of the dot ($s_0 = 1$). The resulting expression is

$$H_{an}(c, \beta, R) = \frac{(1+c^2)}{2c} \kappa(c, \beta, R) M_s, \qquad (2)$$

where $\beta = T/R$ is the aspect ratio of the dot and $\kappa(c, \beta, R)$ is the magnetic stiffness coefficient.

The expression in (2) is plotted as a function of c in Figure 7.*a*, for the geometrical parameters corresponding to the sample S50 (R = 30 nm, T = 50 nm) and using a value for the saturation magnetization $\mu_0 M_S$ = 0.75 T, assumed to be equal to the one measured in a thin film of the same composition.

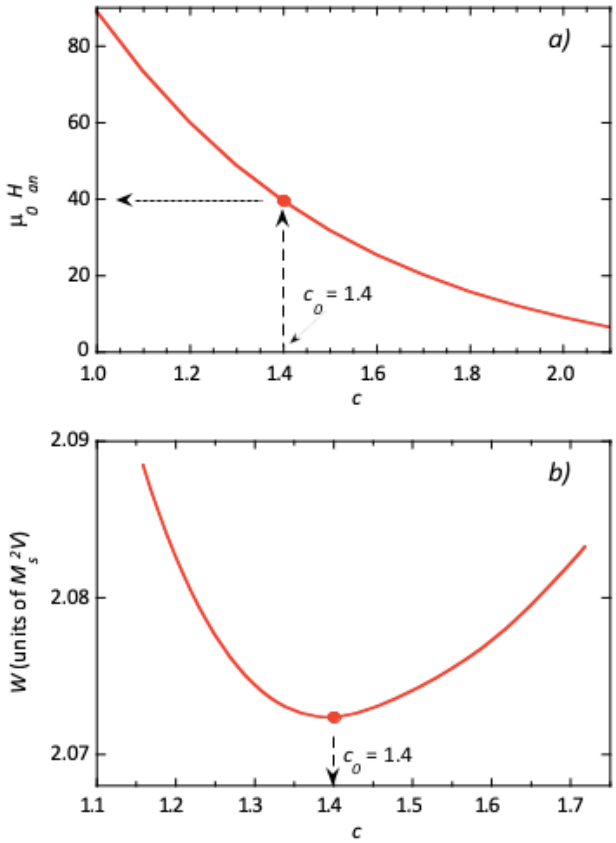

Figure 7. Evaluation of theory results using the data corresponding to sample S50: dot thickness T = 50 nm, radius R = 30 nm, $\mu_0 M_s$ = 0.6 T, $A = 1.3 \times 10^{-11}$ J/m.

a) The vortex annihilation field as function of the reduced vortex core radius *c,* calculated by equation 2 for the case $c > 1$.

b) Magnetic energy calculated by equation 1. The equilibrium value of the vortex core radius *c0* is given by the minimum of the energy. This *c0* value determine the annihilation field for this case to be $\mu_0 H_{an}$ = 40 mT, as shown in the upper plot (*a*).

On the other hand, the equilibrium vortex core radius c_0 can be found by minimizing the magnetic energy $\partial W / \partial c = 0$, calculated with the vortex core situated at the center of the dot (s = 0). Figure 7.*b* represents the dependence of $W(c)$ (calculated with the values corresponding to sample S50). The energy minimum correspond to the equilibrium vortex core radius value of *c0* = 1.4. Using this value in the expression of the annihilation field (Eq. 2 and Figure 7.*a*) we obtain $\mu_0 H_{an}$ = 40 mT, in very good agreement with the measured result.

Discussion

We will analyze the large vortex core state discovered in dots with small radius by comparing the experimental results, the magnetization profiles obtained by the micromagnetic simulations, and the predictions of the theory.

The analytical model that produces Equation (2) has been developed for the case $c > 1$ ($R_C > R$), the *extra-large* vortex core, where the vortex core overflows the limits of the dot. It gives very good results for the sample S50 that seems to be in that situation according to the magnetization profile obtained in the micromagnetic simulations.

The analytical model for the classical magnetic vortex with $c << 1$ ($R_C << R$), where the core radius is negligible, yields the expresion[6]

$$H_{an} = [4\pi F_1(\beta) - (L_e/R)^2]M_s, \qquad (3)$$

where the function $F_1(\beta)$, defined in methods, depends on the aspect ratio of the dot and the shape assumed for the vortex core within the rigid vortex model, and L_e is the exchange length, related with the magnetic exchange stiffness constant. The values of H_{an} obtained from (3) for the classic vortex (c << 1) are essentially larger than those obtained from Eq. (2) for the extra-large core vortex (c > 1). If the core of the vortex is smaller than the dot but is still large ($c < 1$) equation (3) can be adapted as

$$H_{an}(c, \beta, R) = (1 - c)\lfloor 4\pi F_1(\beta) - (L_e/R)^2 \rfloor M_s. \qquad (4)$$

This is the expression that should be, in principle, applicable to samples S30, L30 and L50 which, according to the micromagnetic simulations, are in the case $c < 1$ ($R_C < R$).

The calculated values obtained from equations (2) and (4) for the different samples, together with the experimental and simulated results, are compiled in Table II. The dimensions of the dots are affected by some uncertainty (see Table I), so the theory column of Table II displays values for H_{an} and c calculated using sample parameters within those uncertainties.

Table II. Compilation of the values of the reduced vortex radius (c = Rc/R) and annihilation field Han obtained from magnetic measurements, micro- magnetic simulations and analytical model

sample	measured	simulation		theory[2]		vortex
	$\mu_0 H_{an}$ (mT)	R_c (nm)	$c = R_c/R$	$\mu_0 H_{an}$	c	type[3]
S30	23 ± 2	26 ± 3	0.7 ± 0.1	36 - 41	0.7 - 0.8	L
S50	40 ± 2	36[1]	1.2	40 - 41	0.8 - 1.4	XL/L
L30	63 ± 2	30 ± 4	0.4 ± 0.1	60 - 61	0.5 - 0.6	L
L50	84 ± 2	34 ± 6	0.5 ± 0.1	68 - 70	0.5 - 0.6	L

[1] approximate value obtained by extrapolation (Figure 6.*b*).
[2] range of values obtained within sample size uncertainties (Table I).
[3] L = large vortex core. XL = extra-large vortex core.

For sample S30, equation (4) gives values between 36 and 41 mT, which are significantly larger than experimentally measured value of 23 mT. As explained before, the hysteresis loop of Figure 2.*a* evidence that, although the general behavior is typically vortex-like, the sample present features of in-plane single domain state. This mixed behavior limits the applicability of the analytical model. Alternatively, it is also possible that part of the dots of the sample were actually in in- plane single domain state, due to the closeness of the sample to the frontier in the phase diagram, producing in the measurement an average annihilation field H_{an} smaller than the one that the theory predicts.

The results for sample S50 agrees satisfactorily with the theory behind equation (2) for the extra-large vortex core state in which the vortex core is larger than the dot itself (c > 1).

However, if the inputs to the equation corresponding to the dot size are increased slightly (within the errors given in Table I), the large vortex core state become energetically favorable, giving an equilibrium radius of $c0 = 0.8$, and an annihilation field (using Eq. 4) of $H_{an} = 41$ mT, which is also close to the value measured experimentally. This means that the sample must possibly be close to the crossover from c > 1 (extra-large vortex core state) to c < 1 (large vortex core state). Incidentally, this also demonstrates the continuity between the results given by equation 4 for c < 1 and equation 2 for c > 1. In any case, the size of the vortex core in this sample S50 is significantly larger than those of the other studied samples. While being circularly curled, the magnetization conserves a considerable *z*-component over the whole surface of the dot, which is definitely caused by the proximity the out-of-plane single domain region in the phase diagram. The extra-large vortex core with its enhanced out-of-plane magnetization component makes that the reversal process occur with some coherent rotation of the magnetization as discussed in the experimental results section.

The samples with larger radii, L30 and L50, are properly described in the large vortex core ($c < 1$) framework represented by equation 4. Their calculated equilibrium vortex core radius is approximately half of the dot radius ($c0 \sim 0.5$) in accordance to the experimental MFM measurements and simulated magnetization profiles. The calculated value of the annihilation field for L30 is in rather good agreement with the experiment. Besides, the theory correctly reproduces the observed tendency for H_{an}, although the calculated value for L50 is clearly smaller than the measured one (which can be caused by the strong sensitivity of Eq. 2 and 4 to small variations of c).

Based on the above results, we can conclude that all the examined samples present a large core vortex about 30 nm in radius, but the actual size of the core depends on the aspect ratio of the dot. The vortex core becomes larger for thicker samples, as the sample approaches towards the out-of-plane single domain state (this is graphically observed in Figure 6, where the vortex core of samples S50 and L50 is larger than those of S30 and L30, respectively). In samples with a radius of 30 nm, the large vortex core can result in the development of an extra-large vortex core state, which is proven to be an intermediate stable state between the large vortex core ($c < 1$) and perpendicular single domain state (c >> 1). The magnetization reversal process in this state can accurately be described by the theory that leads to equation 2, whereas the transition from the vortex state to the single domain state, maintaining the axial distribution of the magnetization, was described theoretically in Ref. [30] and, in greater detail in Ref. [20]. The sample S50 ($R = 30$ nm, $T = 50$ nm), which is the one with the largest aspect ratio, is the closest to that extra-large vortex core state. According to the analytical models, this sample is within the range of dot sizes where either the large vortex core ($c < 1$) or the extra-large vortex core ($c > 1$) can be stable (and the other one metastable) simultaneously.

From the point of view of applications, for fabricating small dots with a radius of $R =$ 30 nm, the thickness of sample S50 (50 nm), is probably at the limit for presenting a well-defined vortex magnetization reversal, before approaching to the boundary of the out-of-plane single domain. On the other boundary, the thickness of sample S30 (30 nm) is probably the minimum possible for obtaining clear vortex behavior without the dominance of the in-plane single domain reversal processes.

Conclusions

We have demonstrated experimentally that magnetic circular dots with small radius (R = 30 nm) stick to a magnetic vortex configuration within a thickness range of T = 30 to 50 nm, although the vortex core, that is the region where the magnetization is out of the dot plane, is large compared with the total size of the dot. This has consequences in the magnetization reversal mechanism, and contrasts with the situation in the classical vortex state present in micron-sized dots, where the vortex core can be neglected in describing the magnetization reversal. To the best of our knowledge, this is the first experimental detection of the large-radius-core vortex state in circular magnetic dots. Within the dominant vortex configuration, there are differences between the samples depending on their geometry. The most dramatic case corresponds to the sample S50 (T = 50 nm), where the radius of the core is even larger than the dot radius (extra-large vortex core) as confirmed by micromagnetic simulations and analytic calculations. The sample S30 (T = 30 nm), with a lower aspect ratio, presents a mixture of in-plane single domain state and large vortex core state. Nanodots with larger radius (R = 70 nm), reveal a behavior closer to the classical vortex state, although the large vortex core produces a magnetic configuration that resembles that of a Bloch magnetic skyrmion. The analytical model developed to describe the large vortex core state for either ($R_C > R$) or ($R_C \leq R$), is able to successfully explain the measured vortex annihilation fields. This study experimentally confirms the feasibility of obtaining well-defined vortex behavior in circular dots with radii down to 30 nm, for emerging spintronic and biomedical applications.

Calculation methods

Micromagnetic simulations

We solve the Landau-Lifshits-Gilbert equation for the magnetization motion numerically, which produces the equilibrium configuration of the magnetization for a given geometry, material parameters and applied magnetic field. Micromagnetic simulations were performed with OOMMF software.[27] Although the usual cell size in this kind of simulations is 4 nm, we obtained the same results with smaller cell sizes. To increase the density of points in Figure 6, the data were obtained using cell sizes of 1 nm for samples S30 and S50 (R = 30 nm), and of 2 nm for L30 and L50 (R = 50 nm). The material parameters used in the simulation are the ones commonly used for Permalloy:[5] saturation magnetization $M_S = 8 \times 10^5$ Am^{-1} ($\mu_0 M_S$ = 1 T), exchange constant $A = 1.3 \times 10^{-11}$ Jm^{-1}, no anisotropy. The Gilbert damping coefficient α was set to 0.5 to speed up the calculations. The equilibrium configuration was determined for zero applied field.

Analytical calculations

We use cylindrical coordinates $(\boldsymbol{\rho}, \boldsymbol{\varphi})$ to describe the in-plane radius vector $\boldsymbol{\rho}(\boldsymbol{x}, \boldsymbol{y})$ and assume that the dot magnetization can be averaged over the thickness, that is, over the $\boldsymbol{z}$ coordinate. The position of the vortex core $\mathbf{X} = (\boldsymbol{X}, \boldsymbol{Y})$ in the dot is expressed in reduced variables as $\mathbf{s} = \mathbf{X}/R$. If an external in-plane magnetic field $\boldsymbol{H}$ is applied, then it is convenient to express the dot magnetization as $\mathbf{M}(\boldsymbol{\rho}, \mathbf{X}) = \mathbf{M}(\boldsymbol{\rho} - \mathbf{X})$, assuming that the vortex is rigidly shifted from its equilibrium position at the dot centre.

The total magnetic energy $W = L \int d^2\boldsymbol{\rho} w$ can be decomposed in series on the small parameter $|s| \ll 1$ as

$$W(s) = W(0) + \kappa|s|^2/2 - H\langle M\rangle V, \quad \text{(M1)}$$

where κ is the stiffness coefficient, and $\langle M\rangle$ is the averaged dot magnetization component along the in-plane bias magnetic field H direction.

The problem is reduced to the calculation of the magnetic energy $W(s)$. We use the complex variables $z = (x + iy)/R$ and an analytic function $f(z)$ to describe the displaced vortex. The magnetization components can be expressed as

$$m_x + im_y = \frac{2f(z)}{1+|f(z)|^2}, \quad m_z = \frac{1-|f(z)|^2}{1+|f(z)|^2}. \qquad \text{(M2)}$$

We apply the rigid vortex model $f(z) = e^{i\Phi}0\ (z - s)/c$, which corresponds to the vortex equilibrium skyrmion-like magnetization profile $cos\Theta_0(\rho) = (R^2 - \rho^2)/(R^2 + \rho^2)$. Here, $c = R_c/R \geq 1$ is the reduced vortex core radius (the case of c<<1 was considered by Guslienko et al) and $\phi_0 = C\pi/2$ ($C = \pm 1$ is the vortex chirality).

According to Eq. 1 there are exchange and magnetostatic contributions to the dot magnetic energy of the vortex displaced from the dot center. The exchange contribution to the stiffness coefficient κ is $\kappa_{ex}(c) = -32\pi ATc^2/(1 + c^2)^3$. To calculate the vortex magnetostatic energy w_m we distinguish the energy of the bulk, side surface and face dot surface magnetic charges. The energy cannot be simply expressed via the analytical function $f(z)$. Therefore, we used a direct calculation of w_m via the magnetization bulk and surface divergence, $div\ \mathbf{m}$ and $(\mathbf{m} \cdot \mathbf{n})$ respectively, where the vector $\mathbf{n}$ is normal to the dot surface ($\mathbf{n} = \hat{\boldsymbol{z}}, \hat{\boldsymbol{\rho}}$ for the face and side surface charges, correspondingly). The bulk magnetic charges are absent within the rigid vortex model ($div\ \mathbf{m} = 0$). The magnetostatic energy of the face and side surface charges of the displaced vortex can be calculated by the equation

$$W_m(\mathbf{s}) = \frac{1}{2}\mu_0 M_s^2 \int dS \int dS' \frac{m_n(\mathbf{r},\mathbf{s})m_n(\mathbf{r}',\mathbf{s})}{|\mathbf{r}-\mathbf{r}'|}, \qquad \text{(M3)}$$

where $m_n = (\mathbf{m} \cdot \mathbf{n})$ is the surface divergence.

The side surface charges stiffness coefficient, calculated from Eq. M3, is

$$\kappa_m^s(c,\beta) = 16\pi^2 M_s^2 R^2 T c^2 (1 + c^2)^{-3} F_1(\beta),$$

where

$$F_1(\beta) = \int_0^\infty dt t^{-1} f(\beta t) J_1^2(t), \quad f(x) = 1 - \big(1 - exp(-x)\big)/x,$$

and $\beta = T/R$ is the dot aspect ratio. The face magnetic charges stiffness coefficient is calculated as

$$\kappa_m^f(c,\beta) = 32\pi^2 M_s^2 R^2 T/(\beta c^2) \int_0^\infty dk(1 - \exp(\beta k))\, F(k,c),$$

where the function $F(k,c)$ is given by

$$F(k,c) = 2\left[\int_0^1 d\rho\rho^2 J_1(k\rho)/(1+\tau)^2\right]^2/c^2 + \int_0^1 d\rho\rho J_0(k\rho)(1-\tau)/(1+\tau)\int_0^1 d\rho\rho J_0(k\rho)(\tau-1)/(1+\tau)^3$$

and $\tau = (\rho/c)^2$.

We can write the total stiffness coefficient

$\kappa = \kappa_{ex} + \kappa_m^s + \kappa_m^f$

(in units of M^2V) for the circular dot as

$$\kappa(c,\beta,R) = -16\left(\frac{L_e}{R}\right)^2 \frac{c^2}{(1+c^2)^3} + \frac{16\pi c^2}{(1+c^2)^2}F_1(\beta) + \frac{32\pi}{c^2\beta}\int_0^\infty dk(1-\exp(-\beta k))F(k,c)\ , \quad \text{(M4)}$$

where $L_e = \sqrt{2A/M_s}$ is the exchange length.

Calculating the average in-plane dot magnetization, the Zeeman energy density can be expressed as

$$w_H(s) = -\frac{2c}{1+c^2}HM_s. \quad \text{(M5)}$$

The equilibrium vortex core position displacement s_0 in a small in-plane magnetic field (H) can be calculated from the equation $\partial W/\partial s = 0$ as

$$s_0 = 2cH/\kappa(1+c^2)M_s.$$

Following the paper[6] we consider that the field at which the vortex core center crosses the dot border $s_0 = 1$ should give a good estimation of the vortex annihilation field, H_{an}, for $c > 1$.

$$H_{an}(c,\beta,R) = \frac{(1+c^2)}{2c}\kappa(c,\beta,R)M_s, \quad \text{(M6)}$$

where the stiffness coefficient $\boldsymbol{\kappa(c,\beta,R)}$ is given by Eq. M4.

Conflicts of interest

There are no conflicts of interest to declare.

Acknowledgements

This work has been primarily funded by the Spanish Government under Project MAT2014-55049-C2-R and partially by the Basque Government under the Micro4Fab Project (KK-

2016/00030). The authors wish to express their gratitude to Beatriz Mora for her help with atomic force microscopy measurements. Electron microscopy and magnetic measurements have been performed at SGIKER (UPV/ EHU). K. G. acknowledges support by IKERBASQUE (the Basque Foundation for Science). The work of K. G. was partially supported by Spanish MINECO grants MAT2013-47078-C2-1-P and FIS2016-78591-C3-3-R.

References

1 S.D. Bader, Colloquium: Opportunities in nanomagnetism, *Review of Modern Physics* 78, 2006, 1-15.

2 J. Sinova, I. Zutic, *Nature Materials* **11**, 368–371 (2012)

3 W. F. Brown, *J. Appl. Phys.,* 1968, **39** (2), 993.

4 R. P. Cowburn, D. K. Koltsov, A. O. Adeyeye, M. E. Welland and D. M. Tricker, *Phys. Rev. Lett*., 1999, **83,** 1042–5.

5 W. Scholz, K. Guslienko, V. Novosad, D. Suess, T. Schrefl, R. Chantrell and J. Fidler, *J. Magn. Magn. Mater*, 2003, **266,** 155–63.

6 K. Y. Guslienko, V. Novosad, Y. Otani, H. Shima and K. Fukamichi, *Phys. Rev. B,* 2001, **65**, 024414.

7 B. Pigeau, G. de Loubens, O. Klein, A. Riegler, F. Lochner, G. Schmidt, L.W. Molenkamp, V. S. Tiberkevich and A. N. Slavin, *Appl. Phys. Lett.,* 2010*,* **96,** 132506-3.

8 S. Tsunegi, K. Yakushiji, A. Fukushima, S. Yuasa and H. Kubota, *Appl. Phys. Lett.*, 2016, **109**, 252402.

9 D-H. Kim, E. A. Rozhkova, I. V. Ulasov, S. D. Bader, T. Rajh, M. S. Lesniak and V. Novosad, *Nat. Mater.,* 2010*,* **9**, 165–71.

10 S. Leulmi, X. Chauchet, M. Morcrette, G. Ortiz, H. Joisten, P. Sabon, T. Livache, Y. Hou, M. Carrière, S. Lequien and B. Dieny, *Nanoscale,* 2015*,* **7**, 15904.

11 D-H. Kim, P. Karavayev, E. A. Rozhkova, J. Pearson, V. Yefremenko, S. D. Bader and V. Novosad, *J. Mater. Chem.,* 2011*,* **21**, 8422.

12 A-V. Jausovec, G. Xiong and R. P. Cowburn, *Appl. Phys. Lett.* 2006*,* **88**, 052501-3.

13 T. Shinjo, T. Okuno, R. Hassdorf, K. Shigeto and T. Ono,*Science,* 2000, **289**, 930–2.

14 A. Wachowiak, J. Wiebe, M. Bode, O. Pietzsch, M. Morgenstern and R. Wiesendanger, *Science,* 2002, **298**, 277-3

15 E. K. Semenova, F. Montoncello, S. Tacchi, G. Dürr, E. Sirotkin, E. Ahmad, M. Madami, G. Gubbiotti, S. Neusser, D. Grundler, F. Y. Ogrin, R. J. Hicken, V. V. Kruglyak, D. V. Berkov, N. L. Gorn and L. Giovannini, *Phys. Rev. B,* 2013*,* **87**, 174432-19 .

16 R. K. Dumas, C.-P. Li, I. V. Roshchin, I. K. Schuller and K. Liu, *Phys. Rev. B,* 2007, **75**, 134405-5.

17 I. V. Roshchin, C-P. Li, H. Suhl, X. Batlle, S. Roy, S. K. Sinha, S. Park, R. Pyn, M. R. Fitzsimmons, J. Mejía-López, D. Altbir, A. H. Romero and I. K. Schuller, *EPL,* 2009, **86**, 67008-5 .

18 M. Goiriena-Goikoetxea, A. García-Arribas, M. Rouco, A. V. Svalov and J. M. Barandiaran, *Nanotechnology,* 2016, **27**, 175302-10.

19 S.-H. Chung, R. D. McMichael, D. T. Pierce and J. Unguris, *Phys. Rev. B*, 2010, **81**, 024410

20 K. L. Metlov and K. Y. Guslienko, *J. Magn. Magn. Mater*., 2002, **242–245**, 1015-1017.

21 K. L. Metlov, *J. Appl. Phys*., 2013, **113**, 223905.

22 H. Fredriksson, Y. Alaverdyan, A. Dmitriev, C. Langhammer, D. Sutherland, M. Zäch, and B. Kasemo, *Adv. Mater*.,2007, **19** 4297.

23 W. S. Rasband, ImageJ, U. S. National Institutes of Health, Bethesda, Maryland, USA, http:/imagej.nih.gov/ij/, 1997- 2017.

24 J. Mejía-López, D. Altbir, P. Landeros, J. Escrig, A. H. Romero, I. V. Roshchin, C.-P. Li, M. R. Fitzsimmons, X. Battle and I. Schuller, *Phys. Rev*. B, 2010, **81**, 184417.

25 O. Iglesias-Freire, M. Jaafar, E. Berganza, A. Asenjo, *Beilstein J. Nanotechnol.,* 2016, **7**, 1068–1074.

26 J. Zabaleta, M. Jaafar, A. Asenjo, S. Agramunt-Puig, N. Del- Valle, C. Navau, A. Sanchez, T. Puig, X. Obradors and N. Mestres, *APL Materials*, 2014, **2**, 076111

27 M. J. Donahue and D. G. Porter, **1999** OOMMF user guide, version 1.0 Interagency Report NISTIR 6376 National Institute of Standards and Technology, Gaithersburg, MD Available at (http://math.nist.gov/oommf). Accessed: 22 September 2015.

28 K. Y. Guslienko, *IEEE Magn. Lett*., 2015, **6**, 4000104.

29 A. A. Awad, G. R. Aranda, D. Dieleman, K. Y. Guslienko, G. N. Kakazei, B. Ivanov and F. Aliev, *Appl. Phys. Lett*., 2010 **97**, 132501.

30 K. Y. Guslienko, V. Novosad, *J. Appl. Phys.***,** 2004, **96**, 4451.

31 K. Y. Guslienko, *J. Nanosci. Nanotechnol.,* 2008*,* **8**, 2745-

2760.